Spinodal decomposition of low-density asymmetric nuclear matter

V.Baran[1,2], M. Colonna[1], M. Di Toro[1] and A.B. Larionov[1,3]
[1] *Laboratorio Nazionale del Sud,*
Via S. Sofia 44, I-95123 Catania, Italy
and University of Catania
[2] *IFA, Bucharest, Romania and*
[3] *RRC "I.V. Kurchatov Institute", Moscow 123182, Russia*

We investigate the dynamical properties of asymmetric nuclear matter at low density. The occurrence of new instabilities, that lead the system to a dynamical fragment formation, is illustrated, discussing in particular the charge symmetry dependence of the structure of the most important unstable modes. We observe that instabilities are reduced by charge asymmetry, leading to larger size and time scales in the fragmentation process. Configurations with less asymmetric fragments surrounded by a more asymmetric gas are favoured. Interesting variances with respect to a pure thermodynamical prediction are revealed, that can be checked experimentally. All these features are deeply related to the structure of the symmetry term in the nuclear Equation of State (*EOS*) and could be used to extract information on the low density part of the *EOS*.

PACS numbers: 21.65.+f, 25.70.Pq, 21.60.Ev

I. INTRODUCTION

During the last years the equation of state (EOS) of nuclear matter (NM) has been studied extensively in the symmetric $N = Z$ case. Recent investigations on collisions of radioactive nuclei [1, 2, 3, 4] and on formation and structure of neutron stars [5] have driven the attention to the properties of strongly asymmetric, $N > Z$, nuclear matter. Hence it appears of relevant interest to investigate equilibrium and non-equilibrium features of asymmetric NM and their connection to the used extension of the EOS.

In this work we study the influence of charge asymmetry on the spinodal decomposition ("SD") of nuclear matter at subsaturation density. The "SD" is the growth of small density perturbations, that leads to liquid-gas phase separation, in initially uniform matter located in the low density instability region of the EOS phase diagram. In symmetric nuclear matter, the "SD" was studied extensively in Ref.s [6, 7, 8, 9, 10, 11, 12, 13].

To our knowledge, the first publication on the liquid-gas phase separation in asymmetric (neutron star) matter is Ref. [14], where the coexistence of asymmetric nuclei with a pure neutron gas was predicted, at zero temperature. Recently, the liquid-gas phase transition in asymmetric nuclear matter at finite temperature was studied in Ref.s[15, 16, 17, 18], always in an equilibrium thermodynamical approach. For instance, it was demonstrated in Ref.[15], on the basis of the Quantum Statistical Model, that light clusters emitted from neutron-rich systems have, in average, a larger relative neutron excess than the initial source.

Our discussion is more focussed on non-equilibrium properties of asymmetric nuclear matter and, in particular, on the possibility to observe collective dynamical formation of clusters, with specific mass and charge contents, *on short time scales*. We expect this mechanism to be important in fast expanding systems, as in collisions of beta-unstable nuclei, or as a first step towards preferential equilibrium structures. The latter point, on possible different time scales in the clustering process, will be also addressed in this article.

We consider the unstable growth of density perturbations on the basis of two Vlasov equations, for neutron and proton liquids, coupled through the mean field. The influence of the initial asymmetry on the wave length and growth time of the unstable modes is studied. In neutron-rich NM the formation of larger fragments is favoured and the fragment formation process is delayed in comparison to the case of symmetric NM. The restoration of the isotopic symmetry inside the formed heavy fragments, predicted earlier in Refs. [17, 21], is clearly observed in the "SD" collective dynamical mechanism. Moreover, new non-equilibrium features of the fast clustering processes in asymmetric nuclear systems, that cannot be explained within a thermodynamical approach, are discussed. For instance, for neutron excess systems the proton fraction in the gas phase is expected to be larger when compared to statistical predictions [15]. This effect can be related to the *"freeze-out"* time, preventing the chemical equilibration in the dynamics of heavy ion collisions.

The structure of the article is as follows. In Sect. II a description of the mean-field kinetic approach to the coupled neutron and proton liquids is given. We apply the linear response analysis [6, 7, 8, 9, 10, 11, 12, 13] for the onset of the "SD" instabilities. In parallel, we consider numerical simulations [20] which reproduce all stages of the "SD" evolution, including non-linear effects. Results from analitical and numerical solutions of the coupled Vlasov equations are presented in Sects. III, IV respectively. Summary and conclusions are given in Sect. V.

II. THEORETICAL APPROACH

We start from a mean field description of nuclear dynamics based on two Vlasov equations, for neutron and proton liquids [19, 20, 21], coupled through a self-consistent nuclear field :

$$\frac{\partial f_q(\mathbf{r},\mathbf{p},t)}{\partial t} + \frac{\mathbf{p}}{m}\frac{\partial f_q}{\partial \mathbf{r}} - \frac{\partial U_q(\mathbf{r},t)}{\partial \mathbf{r}}\frac{\partial f_q}{\partial \mathbf{p}} = 0 \ . \tag{1}$$

Here the subscript q stands for n (neutrons) or p (protons) and $f_q(\mathbf{r},\mathbf{p},t)$ is the phase-space distribution function (d.f.). For simplicity, in Eq.(1) we neglect effective mass corrections and the difference between neutron and proton masses, putting $m_n^* = m_p^* = m = 938\ MeV$. Indeed in the low density region studied here we do not expect to have large effective mass corrections. Finally, $U_q(\mathbf{r},t)$ is the self-consistent mean field potential in a Skyrme-like form [21] :

$$U_q = \frac{\delta \mathcal{H}_{pot}}{\delta \rho_q} = A\left(\frac{\rho}{\rho_0}\right) + B\left(\frac{\rho}{\rho_0}\right)^{\alpha+1} + C\left(\frac{\rho'}{\rho_0}\right)\tau_q + \frac{1}{2}\frac{dC(\rho)}{d\rho}\frac{\rho'^2}{\rho_0} - D\triangle\rho + D'\tau_q\triangle\rho' \ , \tag{2}$$

where

$$\mathcal{H}_{pot}(\rho_n,\rho_p) = \frac{A}{2}\frac{\rho^2}{\rho_0} + \frac{B}{\alpha+2}\frac{\rho^{\alpha+2}}{\rho_0^{\alpha+1}} + \frac{C(\rho)}{2}\frac{\rho'^2}{\rho_0} + \frac{D}{2}(\nabla\rho)^2 - \frac{D'}{2}(\nabla\rho')^2 \tag{3}$$

is the potential energy density; $\rho = \rho_n + \rho_p$ and $\rho' = \rho_n - \rho_p$ are respectively the total (isoscalar) and the relative (isovector) density; $\rho_0 = 0.16$ fm^{-3} is the nuclear saturation density; $\tau_q = +1$ ($q = n$), -1 ($q = p$).

The values of the parameters $A = -356.8$ MeV, $B = 303.9$ MeV, $\alpha = 1/6$ and $D = 130$ MeV·fm^5 are adjusted to reproduce the saturation properties of symmetric nuclear matter (binding energy $\epsilon_b = 15.7$ MeV/nucleon at $\rho = \rho_0$, zero pressure at $\rho = \rho_0$, compressibility modulus $K = 201$ MeV) and the surface energy coefficient in the Weizsäcker mass formula $a_{surf} = 18.6$ MeV. We put $D' = 40$ MeV·fm^5 $\sim D/3$ according to Ref.[14], that is also close to the value $D' = 34$ MeV·fm^5 given by the SKM* interaction [22]. Thus, the term $\propto D'$ in the potential energy density (3) favours the growth of isovector density fluctuations [14].

The potential symmetry energy coefficient is equal to: $C(\rho) = C_1 - C_2(\rho/\rho_0)^\alpha$, with $C_1 = 124.9$ MeV and $C_2 = 93.5$ MeV, where the density dependence corresponds to the Skyrme energy density functional of a general kind (c.f. Ref.s[21, 22, 23]). At saturation density the potential symmetry energy coefficient $C(\rho_0) = 31.4$ MeV satisfies the condition [24]:

$$a_{sym} = \frac{\epsilon_F}{3} + \frac{C(\rho_0)}{2} \ ,$$

where $a_{sym} = 28$ MeV is the symmetry energy coefficient in the Weizsäcker mass formula, $\epsilon_F^{eq} = 36.9$ MeV is the Fermi energy for the symmetric system at $\rho = \rho_0$.

As a first step, we apply the linear response analysis to Vlasov Eqs. (1). For a small amplitude perturbation of the d.f., periodic in time, $\delta f_q(\mathbf{r}, \mathbf{p}, t) \sim \exp(-i\omega t)$ we can linearize Eqs. (1) :

$$-i\omega\delta f_q + \frac{\mathbf{p}}{m}\frac{\partial \delta f_q}{\partial \mathbf{r}} - \frac{\partial U_q^{(0)}}{\partial \mathbf{r}}\frac{\partial \delta f_q}{\partial \mathbf{p}} - \frac{\partial \delta U_q}{\partial \mathbf{r}}\frac{\partial f_q^{(0)}}{\partial \mathbf{p}} = 0 \ , \tag{4}$$

where the superscript (0) labels stationary values and δU_q is the dynamical component of the mean field potential. The unperturbed d.f. $f_q^{(0)}$ is in general a Fermi distribution at finite temperature :

$$f_q^{(0)}(\epsilon_p^q) = \frac{1}{\exp\left(\epsilon_p^q - \mu_q)/T + 1\right.} \ , \tag{5}$$

where $\epsilon_p^q = p^2/(2m) + U_q^{(0)}$ and μ_q are respectively energy and chemical potential of the nucleons of type q. In the present work, we neglect finite size effects and consider space-uniform unperturbed d.f. Thus, $\nabla_r U_q^{(0)} = 0$ in Eq. (4) and we consider plane-wave solutions $\delta f_q \propto \exp(-i\omega t + i\mathbf{kr})$. Following a standard Landau procedure [7, 21], one can derive from Eqs. (4) the following system of two equations for neutron and proton density perturbations :

$$[1 + F_0^{nn}\chi_n]\delta\rho_n + [F_0^{np}\chi_n]\delta\rho_p = 0 \ , \tag{6}$$

$$[F_0^{pn}\chi_p]\delta\rho_n + [1 + F_0^{pp}\chi_p]\delta\rho_p = 0 \ , \tag{7}$$

where

$$\chi_q(\omega, \mathbf{k}) = \frac{1}{N_q(T)}\int \frac{2\ d\mathbf{p}}{(2\pi\hbar)^3}\frac{\mathbf{kv}}{\omega + i0 - \mathbf{kv}}\frac{\partial f_q^{(0)}}{\partial \epsilon_p^q} \ , \tag{8}$$

is the long-wave limit of the Lindhard function [7]; $\mathbf{v} = \mathbf{p}/m$;

$$N_q(T) = -\int \frac{2\ d\mathbf{p}}{(2\pi\hbar)^3}\frac{\partial f_q^{(0)}}{\partial \epsilon_p^q} \simeq N_q(0)\left[1 - \frac{\pi^2}{12}\left(\frac{T}{\epsilon_{F,q}}\right)^2\right] \ , \tag{9}$$

is the thermally averaged level density ($N_q(0) = mp_{F,q}/(\pi^2\hbar^3)$, $\epsilon_{F,q} = p_{F,q}^2/(2m)$, $p_{F,q} = \hbar(3\pi^2\rho_q)^{1/3}$) and, finally

$$F_0^{q_1 q_2}(k) = N_{q_1}(T)\frac{\delta U_{q_1}}{\delta \rho_{q_2}} \ , \qquad q_1 = n, p, \qquad q_2 = n, p \tag{10}$$

are the usual zero-order Landau parameters, where the k-dependence is caused by the presence of space derivatives in the potentials (see Eq.(2)). For the particular choice of potentials given by Eq.(2), the Landau parameters are expressed as [25] :

$$F_0^{q_1 q_2}(k) = N_{q_1}(T)\left[\frac{A}{\rho_0} + (\alpha+1)B\frac{\rho^\alpha}{\rho_0^{\alpha+1}} + Dk^2 + (\frac{C}{\rho_0} - D'k^2)\tau_{q_1}\tau_{q_2}\right.$$
$$\left. + \frac{dC}{d\rho}\frac{\rho'}{\rho_0}(\tau_{q_1} + \tau_{q_2}) + \frac{d^2C}{d\rho^2}\frac{\rho'^2}{2\rho_0}\right] \ . \tag{11}$$

The dispersion relation connecting eigenfrequencies to wave vectors can be obtained by taking the determinant of the system (6), (7) equal to zero :

$$(1 + F_0^{nn}\chi_n)(1 + F_0^{pp}\chi_p) - F_0^{np}F_0^{pn}\chi_n\chi_p = 0 \ . \tag{12}$$

Since we are interested in the unstable growth, we put in Eq.(8) $\omega = i\gamma$, where $\gamma > 0$ is the growth rate of the instability. Then, in the particular case of $T = 0$ one can obtain the following simple expression for the Lindhard function (8) (see Ref.[7]) :

$$\chi_q(s_q) = 1 - s_q \arctan(1/s_q) \ , \tag{13}$$

where $s_q = \gamma/(kv_{F,q})$. We stress that without considering the wave number dependence in the Landau parameters (11) one has $\gamma \propto k$ and, hence, an unphysical growth of the short wave length perturbations is favoured [6, 11, 12].

Stability conditions of asymmetric nuclear matter against density fluctuations are derived in the Appendix. The system becomes unstable if at least one of conditions (21), (22) is violated.

The linear technique described above is applicable only in the regime of small-amplitude perturbations, and some relevant results will be shown in the next section. Then as a second step, see Sect. IV, we consider the more powerful numerical solution of the Vlasov Eqs. (1), which is based on the test-particle approach [26, 27]. The detailed description of the numerical method is given in Refs. [20, 28]. In this way, we can also have effects from nonlinear terms and particle collisions. The latter contribution is indeed always present in the dynamical response of heated nuclear matter. However, the main results shown in the next section from a pure mean field approach should not be much affected, since a very dilute system is considered. This will be also confirmed from comparisons with numerical simulations, where the collision integral is included (see Sect. IV).

III. UNSTABLE SOLUTIONS OF EXTENDED LANDAU DISPERSION RELATIONS

We discuss, first, the results of the linear response theory. Fig. 1 shows the instability region (under curves), as given by the inequality:

$$(1 + F_0^{nn})(1 + F_0^{pp}) - F_0^{np}F_0^{pn} < 0 \ , \tag{14}$$

with the Landau parameters taken at $k = 0$ (see the stability condition (22) and text below in the Appendix) in the $\rho - T$ plane for different asymmetries $I = (N - Z)/A$ (a) and in the $\rho - I$ plane for different temperatures (b). The asymmetry leads to shrinking of the spinodal region, reducing both critical temperature and density (Fig. 1a), in agreement with the results of ref.[16]. This is indeed a quite general effect due to the attractive neutron-proton effective interaction and repulsive neutron-neutron and proton-proton ones [19]: a repulsive symmetry term is softening the EOS for asymmetric NM reducing then the low density instability region.

An increasing temperature also reduces the unstable region in the $\rho - I$ plane (Fig.1b).

We have solved the dispersion relation eq.(12) looking at isoscalar growing modes ($\delta\rho_p/\delta\rho_n > 0$), considering various choices of the initial density, temperature and asymmetry of nuclear matter. Fig. 2 reports the growth rate Γ = Im $\omega(k)$ as a function of the wave vector k. The growth rate has a maximum $\Gamma_0 = 0.01 \div 0.03$ c/fm corresponding to a wave vector value around $k_0 = 0.5 \div 1$ fm^{-1} and becomes equal to zero at $k \simeq 1.5k_0$, due to k-dependence of the Landau parameters, as discussed above. One can see also that instabilities are reduced when increasing the temperature. This effect is present also in the symmetric N = Z case [12].

At larger initial asymmetry the development of the "SD" is slower. One should expect also an increasing of the size of the produced fragments due to the "SD" features in asymmetric systems. The effect of the asymmetry on the growth time $t_0 = 1/\Gamma_0$ and on the wave length $\lambda_0 = 2\pi/k_0$ of the most unstable mode is shown in Fig. 3. It is quite clear that the asymmetry dependence of both variables Γ_0 and λ_0 is more pronounced at higher temperature, when the system is closer to the boundary of the spinodal region.

A better understanding of the "SD" in a two-component system can be achieved by studying the chemical composition of the growing mode. On Fig. 4 we show the asymmetry of the perturbation $I_{pt} = (\delta\rho_n - \delta\rho_p)/(\delta\rho_n + \delta\rho_p)$ as a function of the asymmetry of the initially uniform system $I = (\rho_n^{(0)} - \rho_p^{(0)})/(\rho_n^{(0)} + \rho_p^{(0)})$. Without any chemical processes, we should expect $I_{pt} = I$. However, we obtain $I_{pt} \simeq 0.5\ I$. This means that a growing mode produces more symmetric high-density regions (liquid phase) and less symmetric low-density regions (gas phase). Hence, during the "SD", a collective diffusion of protons from low-density regions to high-density regions takes place.

We see from Fig. 4 that the chemical effect becomes stronger with increasing density. This can be explained by the increasing behaviour of the symmetry energy per nucleon with density, in the density region considered here. The effect of increasing the temperature goes in the opposite direction, reducing the chemical effect.

The conclusion is that the fast "SD" mechanism in a neutron-rich matter will dynamically form more symmetric fragments surrounded by a less symmetric gas. Some recent experimental observations from fragmentation reactions with neutron rich nuclei seem to be in agreement with this result on the fragment isotopic content : nearly symmetric Intermediate Mass Fragments (IMF) have been detected surrounded by very neutron-rich light ions [29].

IV. NUMERICAL RESULTS: HEATED NUCLEAR MATTER IN A BOX

The previous analytical study is restricted to the onset of the "SD", in a linearized approach. Then numerical calculations were performed in order to study all stages of the fragment formation process. In the numerical approach we consider nuclear matter in a cubic box of size L imposing periodic boundary conditions. We follow a phase-space test particle method to solve the Landau-Vlasov dynamics, using gaussian wave packets [26, 27, 28]. The dynamics of nucleon-nucleon collisions is included by solving the Boltzmann-Nordheim collision integral using a Monte-Carlo method [27].

We choose the width of the gaussians in order to correctly reproduce the surface energy value in finite systems. In this way a cut-off appears in the short wavelength unstable modes, preventing the formation of too small, unphysical, clusters [12]. In order to have a correct mean field treatment also on the edges of the box, we have used a self-consistent *stuffing* method, filling a layer of $6fm$ thickness all around the box with test particles having symmetric positions with respect to those on the opposite side in the box.

The calculations were performed using 80 gaussians per nucleon and the number of nucleons inside the box was fixed in order to reach the initial uniform density value. An initial temperature is introduced by distributing the test particle momenta according to Fermi d.f. (Eq. (5)). We have checked that we reproduce at equilibrium the right "EOS" corresponding to the used effective forces (see Sect. II).

We have followed the space-time evolution of test-particles in the box with side $L = 24fm$ for three values of the initial asymmetry $I = 0,\ 0.25$ and 0.5, at initial density $\rho^{(0)} = 0.4\rho_0$ and temperature $T = 5$ MeV. The initial density perturbation was created automatically due to the random choice of test-particle positions. Results for the initial asymmetries $I = 0$ and $I = 0.5$, are reported in Fig. 5, (a) and (b) respectively. Figure 5 shows density distributions in the plane $z = 0$, which contains the center of the box, at three time steps $t = 0,\ 100$ and 200 fm/c, corresponding respectively to initial conditions, intermediate and final stages of the "SD". Clearly, the growth of the small initial density perturbations takes place.

We have compared the dynamical evolution, as given by the test particle method, with the analytical predictions of Sect. III (Figs. 2-4). To do this, two variables were constructed: the total density variance (see [9])

$$\sigma = < (\rho - \rho^{(0)})^2 >_{all} \tag{15}$$

and the correlation function between proton and neutron density perturbations, normalized to the neutron density variance,

$$R_{pn} = \frac{< (\rho_p - \rho_p^{(0)})(\rho_n - \rho_n^{(0)}) >_{all}}{< (\rho_n - \rho_n^{(0)})^2 >_n} \ . \tag{16}$$

In Eqs. (15),(16) $< ... >_{all}$ denotes the average over all test particles, while $< ... >_n$ denotes the average over neutrons only. The densities ρ, ρ_n and ρ_p were calculated in the position of the test particle considered by taking contributions from gaussians of all test particles. For a dominant plane-wave perturbation we have:

$$\begin{aligned} \sigma &\propto \exp(2\Gamma t), \\ R_{pn} &= \frac{\delta\rho_p}{\delta\rho_n} \ . \end{aligned}$$

Fig. 6 shows the evolution of σ (a) and of the (test-particle) perturbation asymmetry $I_{pt} = (1 - R_{pn})/(1 + R_{pn})$ (b), for the same initial conditions discussed above, i.e. $T = 5\ MeV$, $\rho^{(0)} = 0.4\rho_0$ and asymmetries $I = 0.0,\ 0.25,\ 0.5$.

A general feature is the clear linear increase of $ln(\sigma)$ in the time interval $50 < t < 150$ fm/c. During the first 50 fm/c the system is quickly "self-organizing" selecting the most unstable normal mode. Afterwards the variance (Eq. (15)) increases exponentially with a time scale given by $\Gamma = \mathrm{Im}\ \omega(k)$. In correspondence (see Fig.6b), the perturbation asymmetry I_{pt} reveals also a quick saturation at $t \sim 50$ fm/c. At earlier times the proton and neutron density perturbations are not correlated, but at $t > 50$ fm/c the correlation of plane-wave type ($\delta\rho_p/\delta\rho_n = \mathrm{const} > 0$) develops.

We notice that the time scales necessary to reach the asymmetry value characteristic of the most important growing modes, that are quite short in our calculations, generally depend on the structure of the initial noise put in the neutron

and proton densities. In our calculations all modes are nearly equally excited. This causes the quick appearance of the features associated with the dominant mode. In agreement with analytical calculations, the instability grows slower in the case of larger asymmetry.

For an initial asymmetry $I = 0.5$, the extracted values of growth time $\Gamma \simeq 0.01$ c/fm and perturbation asymmetry $I_{pt} \simeq 0.24$ (see Fig. 6), and of wave length $\lambda \simeq 12$ fm (from the distance between the density distribution maxima in Fig. 5b), are in good agreement with the analytical results presented in Figs. 3,4.

The "SD" leads to a fast formation of the liquid (high density) and gaseous (low density) phases in the matter. Indeed this dynamical mechanism of clustering will roughly end when the variance (Eq. (15)) saturates [30], i.e. around 250 fm/c in the asymmetric cases (see Fig. 6a).

We will discuss in the following the "chemistry" of the liquid phase formation. In Fig. 7 we report the time evolution of neutron (thick histogram in Fig. 7a) and proton (thin histogram in Fig. 7a) abundances and asymmetry (Fig. 7b) in various density bins. The dashed line respectively shows the initial uniform density value $\rho \simeq 0.4\rho_0$ (Fig. 7a) and the initial asymmetry $I = 0.5$ (Fig. 7b). The drive to higher density regions is clearly different for neutrons and protons: at the end of the dynamical clustering mechanism we have very different asymmetries in the liquid and gas phases (see the panel at $250fm/c$ in Fig. 7b).

It was shown in Refs. [14, 16, 17], on the basis of thermodynamics, that the two phases should have different asymmetries, namely, $I_{gas} > I_{liquid}$, and actually a pure neutron gas was predicted at zero temperature if the initial global asymmetry is large enough ($I > 0.4$) [14]. Here we are studying this chemical effect in a non-equilibrium clustering process, on very short time scales. The interest is in the observation of new features, not expected in a thermodynamical picture.

In our numerical model, we divide the system into liquid-like and gas-like phases as follows. The i-th test particle belongs to the liquid- (gas-) like phase if $\rho_i > (<)\ \rho(t = 0)$, where ρ_i is the total density in the position of the i-th test particle, $\rho(t = 0)$ is the initial density [31].

Fig. 8 presents the time evolution of the asymmetry in liquid and in gas. Strong fluctuations take place at the beginning of the evolution. However, at $t > 50$ fm/c, results are quite stable. In the symmetric case ($I = 0$), both liquid and gas keep the symmetry in the course of the time evolution. *However for non-zero initial asymmetry liquid becomes more symmetric and gas less symmetric (neutron-rich) as time goes.* The asymmetry in liquid and gas phases saturates rather early, at $t = 200 \div 300$ fm/c, just on the time scale of dynamical clusterization.

This suggests an evidence of a two-stage fragment formation process. On the first stage, the fast "SD" takes place ($t < 250$ fm/c, see Fig. 6a). At the end of this stage, due to reduced asymmetry of the perturbation, see Fig. 4, liquid acquires a lower asymmetry and gas acquires a higher one. On the second stage ($t > 250$ fm/c) we have a statistical nucleation process: protons and neutrons diffuse very slowly from gas to liquid, see Fig. 9a, with approximately equal rates (Fig. 9b). Since the gas is already highly asymmetric and the liquid is more close to symmetry, this diffusion process leads to a further growth of asymmetry in the gas and does not change the asymmetry of the liquid. Eventually, on long time scales, we can expect to reach the thermodynamical limit of Refs. [14, 16, 17], i.e. an almost pure neutron gas.

From our dynamical analysis we can conclude that the second slow mechanism for liquid formation is certainly present in a confined system and will be stopped in an expanding case. We deduce that the isotopic contents of the gas phase could give a measure of the "*freeze-out*" time: a very neutron-rich gas will correspond to a slowly expanding nuclear system.

This effect is quantitatively shown in Fig. 10 where we present asymmetries of the two phases at different time stages, as given by the test-particle simulations. We choose two "*freeze-out*" times, one corresponding to the intermediate stage of the "SD" ($t = 150$ fm/c) and the second inside the slow diffusion process ($t = 400$ fm/c). The first choice of freeze-out time is close to the time scale of the fast multifragment breakup in intermediate energy heavy ion collisions (c.f. [12, 30, 32]).

The asymmetry of the liquid is, practically, not dependend on the choice of "*freeze-out*" time. On the contrary, the asymmetry of the gas and the number of gas particles are very sensitive to this choice.

V. SUMMARY AND CONCLUSIONS

An investigation of fragment formation through Spinodal Decomposition in low-density asymmetric nuclear matter has been performed. Important information on the early evolution of the unstable modes is obtained performing an analytical linear analysis to the Vlasov equations, for neutron and proton liquids, coupled through the mean field. Then a numerical study of nuclear systems with periodic boundary conditions has been applied to describe all stages of the fragment formation process.

We have shown that charge asymmetry changes time and space scales of the fragment formation process. This effect could be observed experimentally.

With respect to the fragment isotopic distribution, we predict that the "SD" in asymmetric systems is accompanied by a collective diffusion of protons from low to high density regions. Thus the produced heavy fragments will be more symmetric than the initial uniform system. This qualitatively corroborates earlier thermodynamical studies [17]. However the chemical composition of fragments is established just after the finishing of the fast "SD" stage. Hence it is essentially defined by the non-equilibrium mean field dynamics and a thermodynamical approach gives only a rough schematic description of this process, with a slow nucleation component likely absent in fragmentation reactions with radioactive beams. In general in a dynamical multifragmentation process with neutron rich systems we expect a proton fraction in the gas phase, i.e. among emitted nucleons and light clusters, larger than the thermodynamical prediction.

Finally we think that different choices of effective interaction, (eg. with different density dependence in the symmetry energy coefficient $C(\rho)$) will support the qualitative conclusions of our work, since all realistic effective interactions give a similar behaviour for the potential symmetry energy per nucleon in the region of subnuclear densities [33]. However the size of the instability region and the isotopic structure of the most unstable collective modes will be certainly dependent on the used effective force. Therefore, considering fragmentation reactions with radioactive beams, it would be possible to extract important information on the low density part of the EOS in asymmetric nuclear matter, of large interest for the understanding of life and structure of neutron stars.

Acknowledgements

We gratefully acknowledge intense and stimulating discussions within the $ISO-DYN$ working group, international working group on isospin effects on nuclear dynamics. Two of us, V.B. and A.B.L., acknowledge kind hospitality and financial support of LNS-INFN.

This work was supported in part by the Commission of the European Community, under Contract No. ERBFMB I-CT-960654.

Appendix: Stability conditions

Here we derive the stability conditions of asymmetric nuclear matter against density perturbations. Let us write down the variation of the free energy density $\mathcal{F} = \epsilon - T\sigma$, where ϵ and σ are respectively energy and entropy densities, over proton and neutron densities, up to the second order [14] keeping constant temperature and volume :

$$\delta\mathcal{F} = \mu_n\delta\rho_n + \mu_p\delta\rho_p + \frac{\partial\mu_n}{\partial\rho_n}\frac{\delta\rho_n^2}{2} + \frac{\partial\mu_p}{\partial\rho_p}\frac{\delta\rho_p^2}{2} + \frac{\partial\mu_p}{\partial\rho_n}\delta\rho_n\delta\rho_p \ . \tag{17}$$

First two terms disappear after integration over the volume, since the total neutron and proton numbers are conserved :

$$\int d^3r\delta\mathcal{F} = \frac{1}{2}\int d^3r\left[\frac{\partial\mu_n}{\partial\rho_n}\delta\rho_n^2 + \frac{\partial\mu_p}{\partial\rho_p}\delta\rho_p^2 + 2\frac{\partial\mu_p}{\partial\rho_n}\delta\rho_n\delta\rho_p\right] \ . \tag{18}$$

In order the system to be stable against density fluctuations, the quadratic form in square brackets of eq. (18) must be positive defined. Thus, we obtain two stability conditions :

$$\frac{\partial\mu_n}{\partial\rho_n} > 0 \quad \text{or} \quad \frac{\partial\mu_p}{\partial\rho_p} > 0 \ , \tag{19}$$

$$\frac{\partial\mu_n}{\partial\rho_n}\frac{\partial\mu_p}{\partial\rho_p} - \left(\frac{\partial\mu_p}{\partial\rho_n}\right)^2 > 0 \ . \tag{20}$$

The system is unstable if at least one condition is violated. We notice that it is enough to satisfy only one inequality in (19), since the other one will be satisfied automatically, if condition (20) is fulfilled. In an equivalent way, the stability conditions (19) and (20) can be expressed in terms of the Landau parameters as follows :

$$1 + F_0^{nn} > 0 \quad \text{or} \quad 1 + F_0^{pp} > 0 \ , \tag{21}$$

$$(1 + F_0^{nn})(1 + F_0^{pp}) - F_0^{np}F_0^{pn} > 0 \ , \tag{22}$$

where we have used the relation

$$N_q(T)\frac{\partial\mu_q}{\partial\rho_{q'}} = \delta_{qq'} + F_0^{qq'}, \qquad q = n, p \qquad q' = n, p \tag{23}$$

with $\delta_{qq'} = 1$ if $q = q'$ and $\delta_{qq'} = 0$ if $q \neq q'$. The relation (23) is obtained by considering the variation over $\delta\rho_{q'}$ of both sides of the equation:

$$\rho_q = \int \frac{2\ d\mathbf{p}}{(2\pi\hbar)^3} f_q^{(0)}(\epsilon_p^q)\ . \tag{24}$$

In the case of the interaction used here (see Eq. (11)), the condition (21) is always satisfied.

The stability condition (20) was derived first in Ref. [14]. Then it was shown in Ref. [16] that this stability condition can be rewritten equivalently as:

$$\left(\frac{\partial P}{\partial \rho}\right)_{T,y} \left(\frac{\partial \mu_p}{\partial y}\right)_{T,P} > 0\ , \tag{25}$$

where $y = \rho_p/\rho$ is the proton fraction, $P = \rho \left(\frac{\partial \mathcal{F}}{\partial \rho}\right)_{T,y} - \mathcal{F}$ is the pressure.

The boundary of the instability region can be obtained just putting $\omega = 0$ in the Lindhard function (8). Since $\chi_q(\omega = 0, k) = 1$, we have from dispersion relation (12) :

$$(1 + F_0^{nn})(1 + F_0^{pp}) - F_0^{np} F_0^{pn} = 0\ . \tag{26}$$

In the case of symmetric nuclear matter ($F_0^{nn} = F_0^{pp},\ F_0^{np} = F_0^{pn}$) the stability conditions (21),(22) are equivalent to the system of Pomeranchuk stability criteria [6] for isoscalar and isovector motions :

$$1 + F_0 > 0\ , \tag{27}$$

$$1 + F_0' > 0\ , \tag{28}$$

where $F_0 \equiv F_0^{nn} + F_0^{np}$ and $F_0' \equiv F_0^{nn} - F_0^{np}$ are the isoscalar and the isovector Landau parameters [24].

[1] R. Pak et al., Phys. Rev. Lett. **78** (1996) 1022; ibid. p. 1026.
[2] B.A. Li, C.M. Ko and Z.Z. Ren, Phys. Rev. Lett. **78** (1996) 1644.
[3] K.E. Zyromski et al., Phys. Rev. C **55** (1997) R562.
[4] L.G. Sobotka et al., Phys. Rev. C **55** (1997) 2109.
[5] Madappa Prakash et al., Phys. Rep. **280** (1997) 1.
[6] C.J. Pethick and D.G. Ravenhall, Nucl. Phys. A **471** (1987) 19c.
[7] C.J. Pethick and D.G. Ravenhall, Ann. Phys. (N.Y.) **183** (1988) 131.
[8] H. Heiselberg, C.J. Pethick and D.G. Ravenhall, Ann. Phys. **223** (1993) 37.
[9] M. Colonna, M. Di Toro, A. Guarnera, V. Latora and A. Smerzi, Phys. Lett. **307** (1993) 273.
[10] M. Colonna, Ph. Chomaz and J. Randrup, Nucl. Phys. A **567** (1994) 637.
[11] A.B. Larionov and I.N. Mishustin, Phys. of At. Nucl. **57** (1994) 636.
[12] M. Colonna and Ph. Chomaz, Phys. Rev. C **49** (1994) 1908.
[13] L.P. Csernai, J. Nèmeth and G. Papp, APH Heavy Ion Physics **3** (1996) 17.
[14] Gordon Baym, Hans A. Bethe and Christopher J. Pethick, Nucl. Phys. A **175** (1971) 225.
[15] Jens Konopka, Harald Graf, Horst Stöcker, and Walter Greiner, Phys. Rev. C **50** (1994) 2085.
[16] Horst Müller and Brian D. Serot, Phys. Rev. C **52** (1995) 2072.
[17] Bao-An Li, C.M. Ko, Nucl. Phys. A **618** (1997) 498.
[18] S. Ray, J. Shamanna, T.T.S. Kuo, Phys. Lett. B **392** (1997) 7.
[19] P. Haensel, Nucl. Phys. A **301** (1978) 53.
[20] V. Baran, M. Bassi, A. Bonasera, M. Di Toro and S. Maccarone *Zero- to first-sound transition for isovector modes in heated nuclear matter*, Preprint LNS, Sept. 1997, submitted to Phys. Rev. C
[21] M. Colonna, M. Di Toro and A.B. Larionov, *Collective modes in asymmetric nuclear matter* , Preprint LNS, Sept. 1997, submitted to Phys. Lett. B
[22] H. Krivine, J. Treiner and O. Bohigas, Nucl. Phys. A **336** (1990) 155.
[23] K. Sumiyoshi et al., Nucl. Phys. A **552** (1993) 437.
[24] A.B. Migdal, *Theory of Finite Fermi systems and Applications to Atomic Nuclei* (Interscience, London, 1967).
[25] The most general expression (see Eq.(5) in Ref.[19]) for the quasiparticle interaction amplitude should include also a term, caused by the Coulomb interaction, $\propto (\tau_{q_1} - \tau_{q_2})$, which does not conserve the total isospin of the colliding quasiparticles. In our work we drop this term for simplicity.
[26] Ch. Gregoire et al., Nucl. Phys. A **465** (1987) 315.
[27] A. Bonasera, F. Gulminelli and J. Molitoris, Phys. Rep. **243** (1994) 1.
[28] V. Baran, A. Bonasera, M. Colonna, M. Di Toro and A. Guarnera, Prog. Part. Nucl. Phys. **38** (1997) 263.
[29] S. Yennello, "Isotopic information in the fragment resulting from intermediate energy heavy ion collisions" in Proc. Int. School-Seminar on "Heavy Ion Physics", Ed. Yu. Ts. Oganessian, World Sci. 1997 and private communication.
[30] M. Colonna, M. Di Toro and A. Guarnera, Nucl. Phys. A **580** (1994) 312
[31] These parts become real phases at the late stage of the "SD" ($t > 200\ fm/c$). However below, for brevity, we call liquid- (gas-) like part as liquid (gas) during all the evolution.
[32] A.S. Botvina, A.B. Larionov, I.N. Mishustin, Yad. Fiz. **58** (1995) 1803.
[33] I. Bombaci, in *Perspectives on Theoretical Nuclear Physics*, edited by S. Rosati et al. (ETS-Pisa, 1996), p. 223.

Figure captions

Fig. 1 Spinodal boundaries in density-temperature plane at different asymmetries (a) and in density-asymmetry plane at different temperatures (b). Instability regions are under curves.

Fig. 2 Growth rate of instability as a function of the wave vector, as calculated from the dispersion relation (12) for $\rho = 0.2\rho_0$, $T = 5$ MeV (short-dashed lines); $\rho = 0.4\rho_0$, $T = 5$ MeV (solid lines); and $\rho = 0.4\rho_0$, $T = 10$ MeV (long-dashed lines). Lines are labeled with the asymmetry value I.

Fig. 3 Wave length λ_0 (a) and growth time t_0 (b) of the most unstable mode as a function of the asymmetry I for $\rho^{(0)} = 0.2\rho_0$ (dashed lines) and $\rho^{(0)} = 0.4\rho_0$ (solid lines). Lines are labeled with the temperature T in MeV.

Fig. 4 Perturbation asymmetry I_{pt} versus initial asymmetry I for different initial densities and temperatures : $\rho^{(0)} = 0.4\rho_0$ and $T = 5$ MeV (solid line), $\rho^{(0)} = 0.2\rho_0$ and $T = 5$ MeV (short-dashed line), $\rho^{(0)} = 0.2\rho_0$ and $T = 10$ MeV (long-dashed line).

Fig. 5 Time evolution of the density $\rho(x, y)$ in the plane $z = 0$ as given by the test particle code for initial density $\rho^{(0)} = 0.4\rho_0$, at temperature $T = 5$ MeV and asymmetries $I = 0$ (a) and $I = 0.5$ (b). Upper panels show contour plots of the function $\rho(x, y)$ and lower panels report the corresponding two-dimensional surfaces. The density is in units of fm^{-3} x 10^3.

Fig. 6 Time dependence of the density variance (a) and of perturbation asymmetry (b) (see text for definitions) in test particle simulations at initial density $\rho^{(0)} = 0.4\rho_0$ and temperature $T = 5$ MeV for initial asymmetries $I = 0$, 0.25 and 0.5 (solid, long- and short-dashed lines respectively). The straight lines on Fig. 6a show linear fits to the initial stage of the SD.

Fig. 7 Time evolution of neutron (thick solid lines) and proton (thin solid lines) abundances (a) and asymmetry (b) in different density bins. Calculations refer to the case with initial temperature $T = 5$ MeV. Initial values of density $\rho^{(0)} = 0.4\rho_0$ and asymmetry $I = 0.5$ are indicated by dashed lines.

Fig. 8 Time evolution of asymmetries in liquid (solid lines) and in gas (long-dashed lines) for initial asymmetries (shown by short-dashed lines) $I = 0$, 0.25 (a) and $I = 0$, 0.5 (b).

Fig. 9 Ratio of total number of particles in gas to total number of particles in liquid (a) and number of neutrons and protons in gas (b) versus time.

Fig. 10 Asymmetries in gas (squares) and in liquid (circles) as functions of the initial asymmetry. Long-dashed (solid) lines correspond to the "*freeze-out*" time 400 (150) fm/c. In the liquid phase there is no appreciable difference between the two lines.

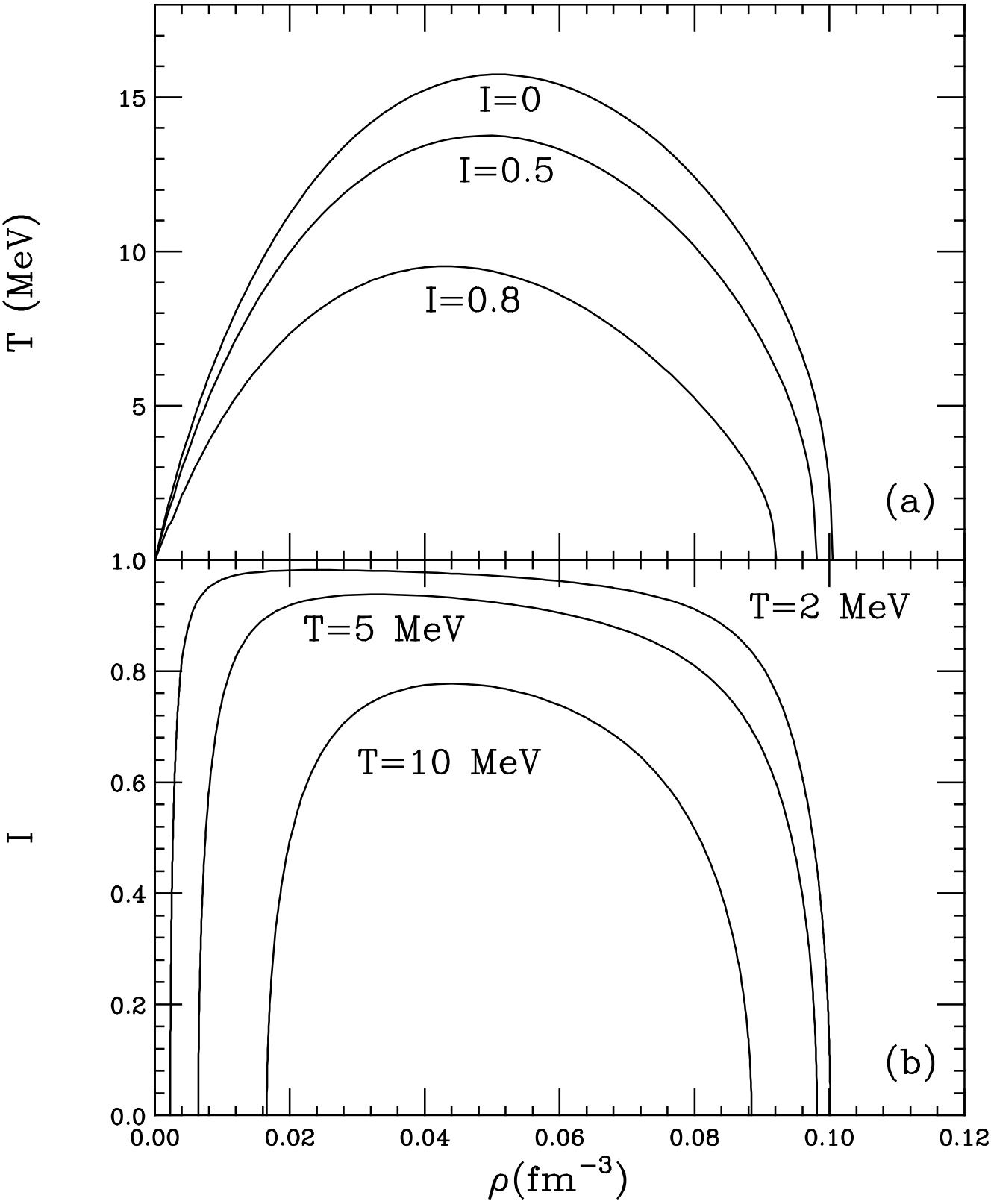
T (MeV)
15
10
5
1.0
I=0
I=0.5
I=0.8
(a)
T=2 MeV
T=5 MeV
T=10 MeV
I
0.8
0.6
0.4
0.2
0.0
(b)
0.00
0.02
0.04
0.06
0.08
0.10
0.12
ρ(fm^-3)

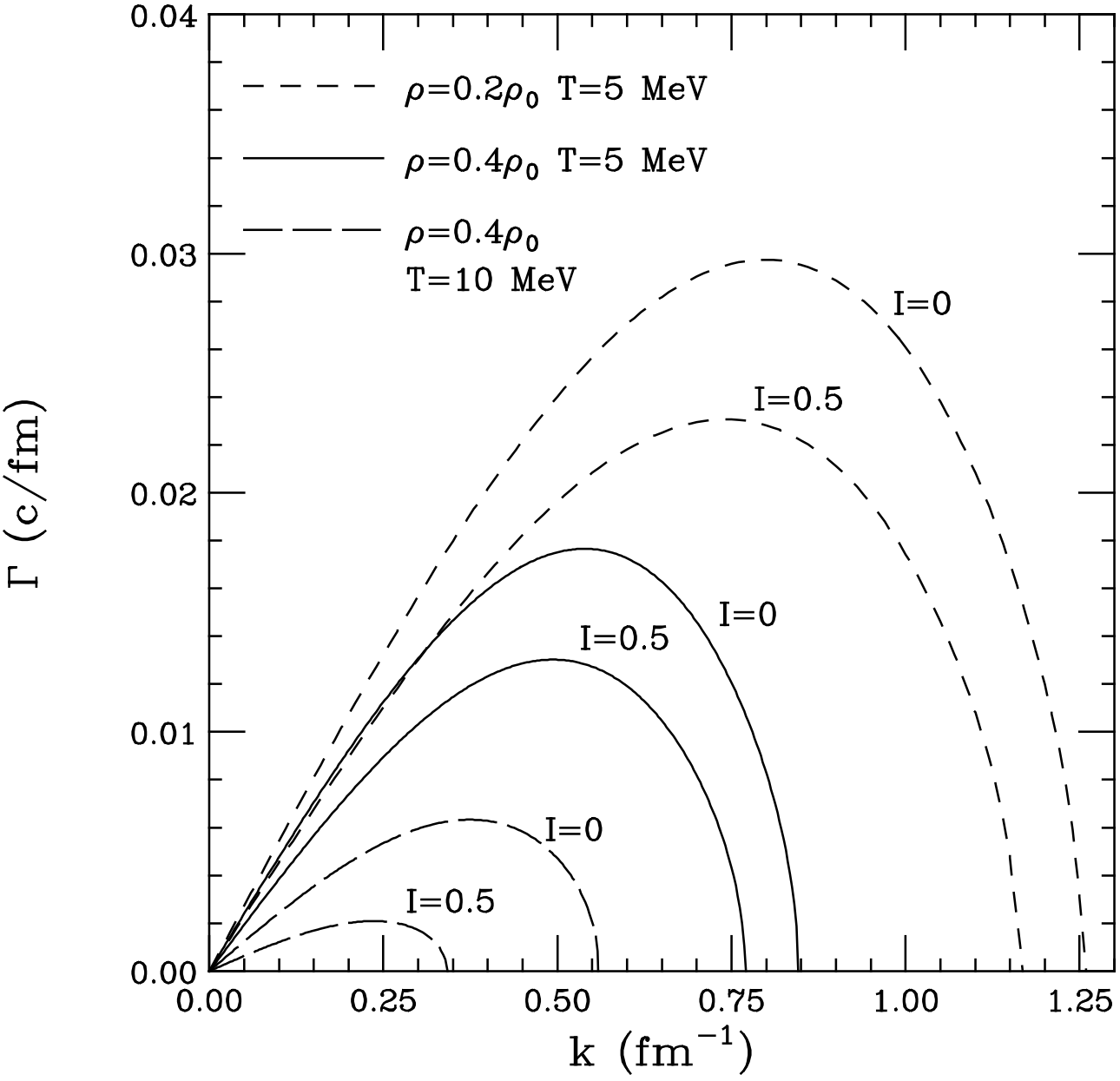
0.04
0.03
0.02
0.01
0.00
Γ (c/fm)
ρ=0.2ρ0 T=5 MeV
ρ=0.4ρ0 T=5 MeV
ρ=0.4ρ0
T=10 MeV
I=0
I=0.5
I=0
I=0.5
I=0
I=0.5
0.00
0.25
0.50
0.75
1.00
1.25
k (fm−1)

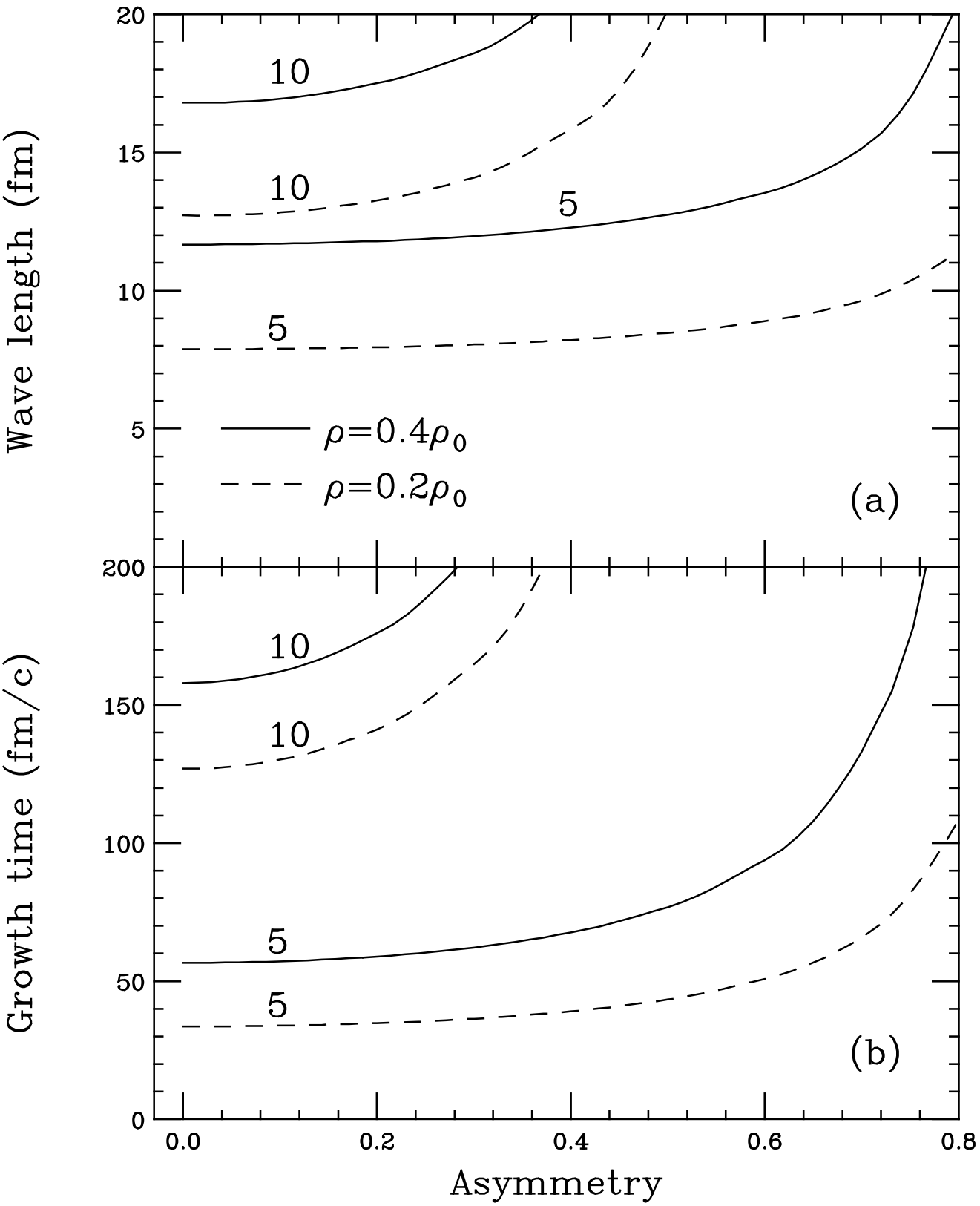
Wave length (fm)
Growth time (fm/c)
Asymmetry
10
10
5
5
$\rho=0.4\rho_0$
$\rho=0.2\rho_0$
(a)
(b)
20
15
10
5
200
150
100
50
0
0.0
0.2
0.4
0.6
0.8

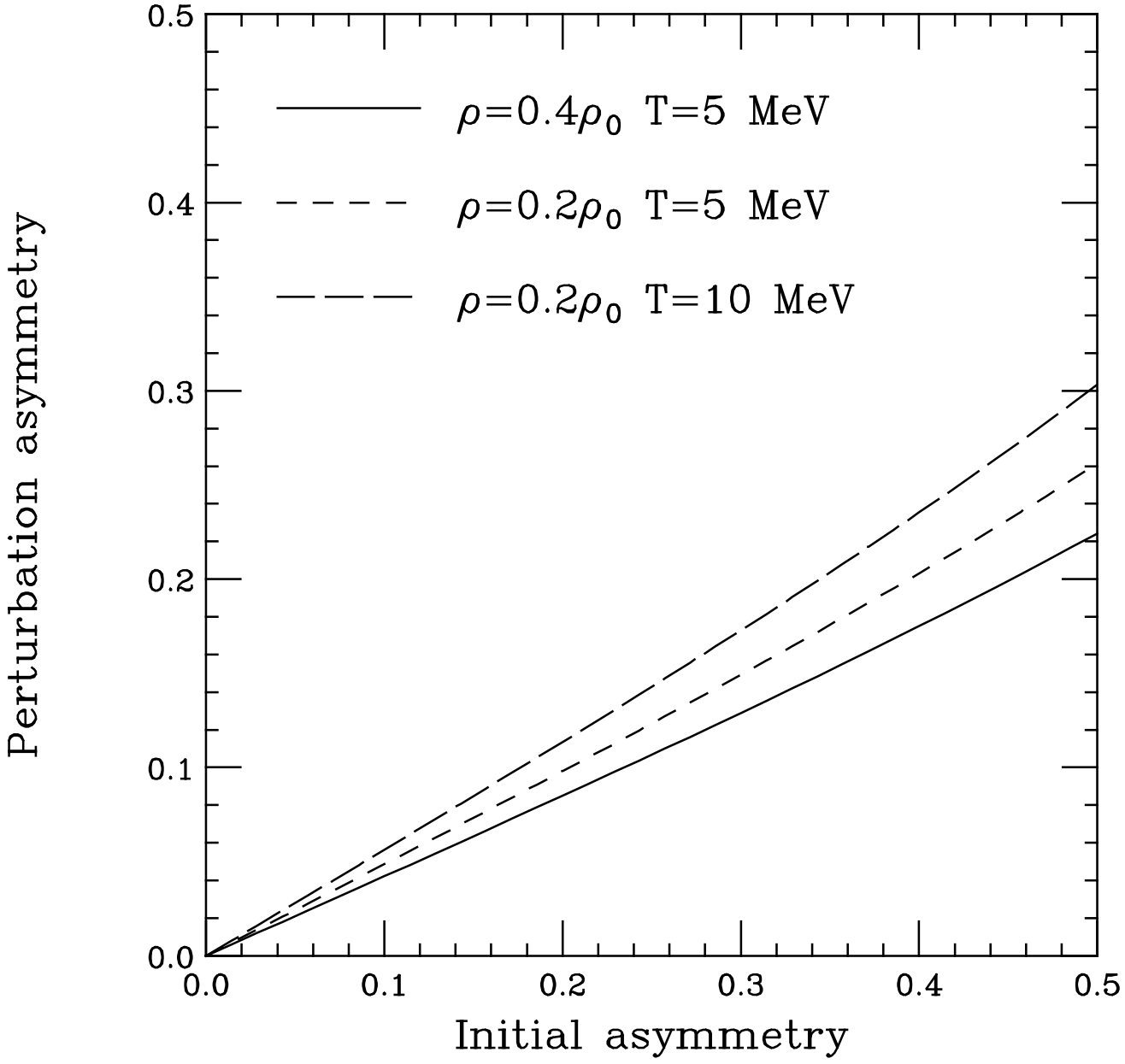
0.5
0.4
0.3
0.2
0.1
0.0
0.0
0.1
0.2
0.3
0.4
0.5
Perturbation asymmetry
Initial asymmetry
ρ=0.4ρ0 T=5 MeV
ρ=0.2ρ0 T=5 MeV
ρ=0.2ρ0 T=10 MeV

(a)
density
150
100
50
x (nm)
y (μm)

(b)

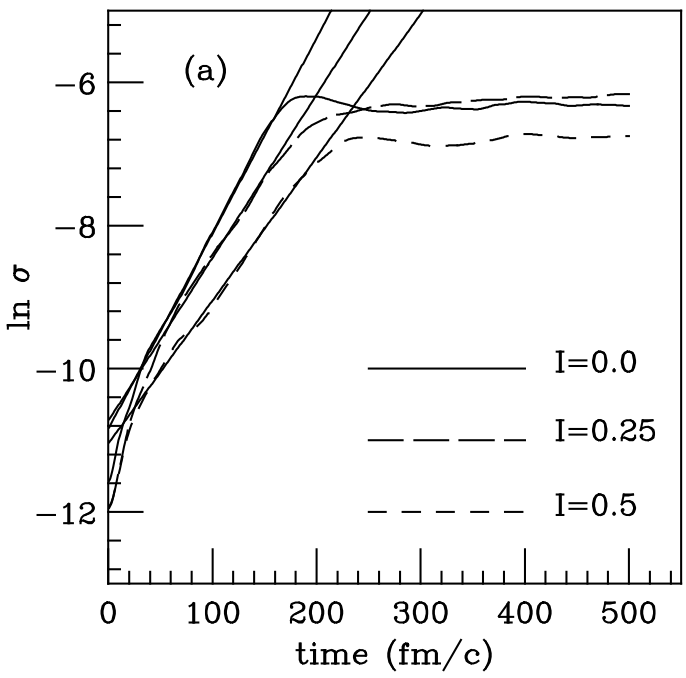
(a)
ln σ
−6
−8
−10
−12
I=0.0
I=0.25
I=0.5
0
100
200
300
400
500
time (fm/c)

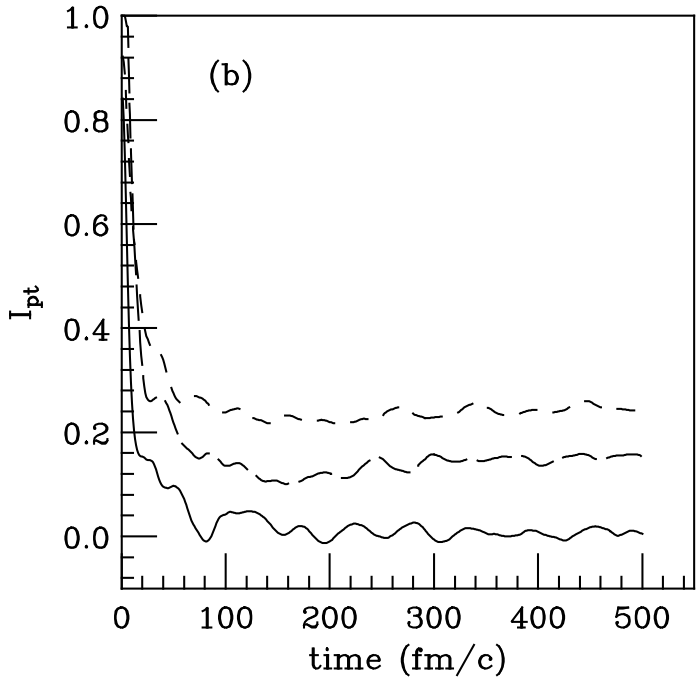
(b)
I_{pt}
1.0
0.8
0.6
0.4
0.2
0.0
0
100
200
300
400
500
time (fm/c)

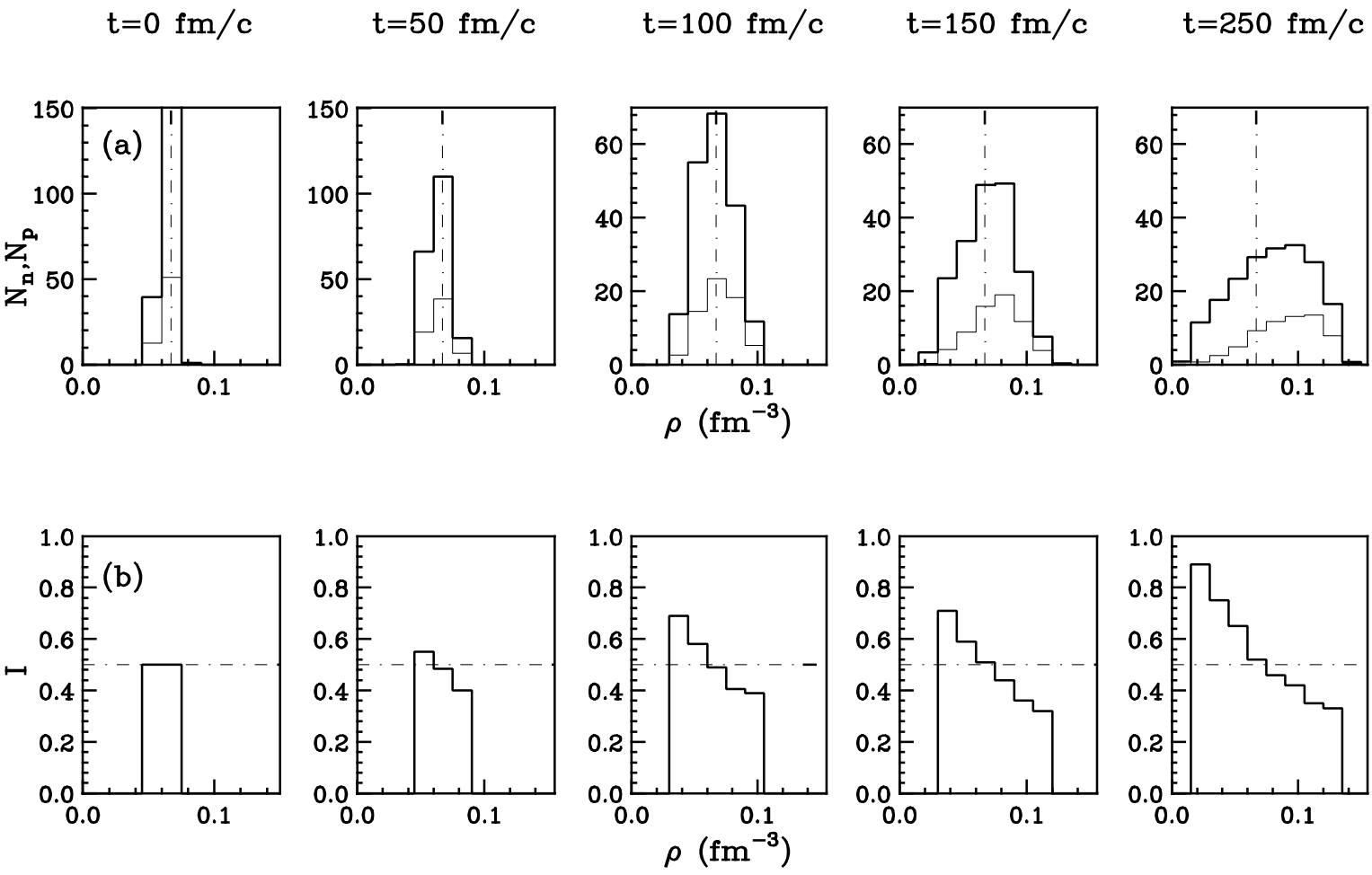
t=0 fm/c
t=50 fm/c
t=100 fm/c
t=150 fm/c
t=250 fm/c
(a)
(b)
N_n, N_p
I
ρ (fm^{-3})
ρ (fm^{-3})

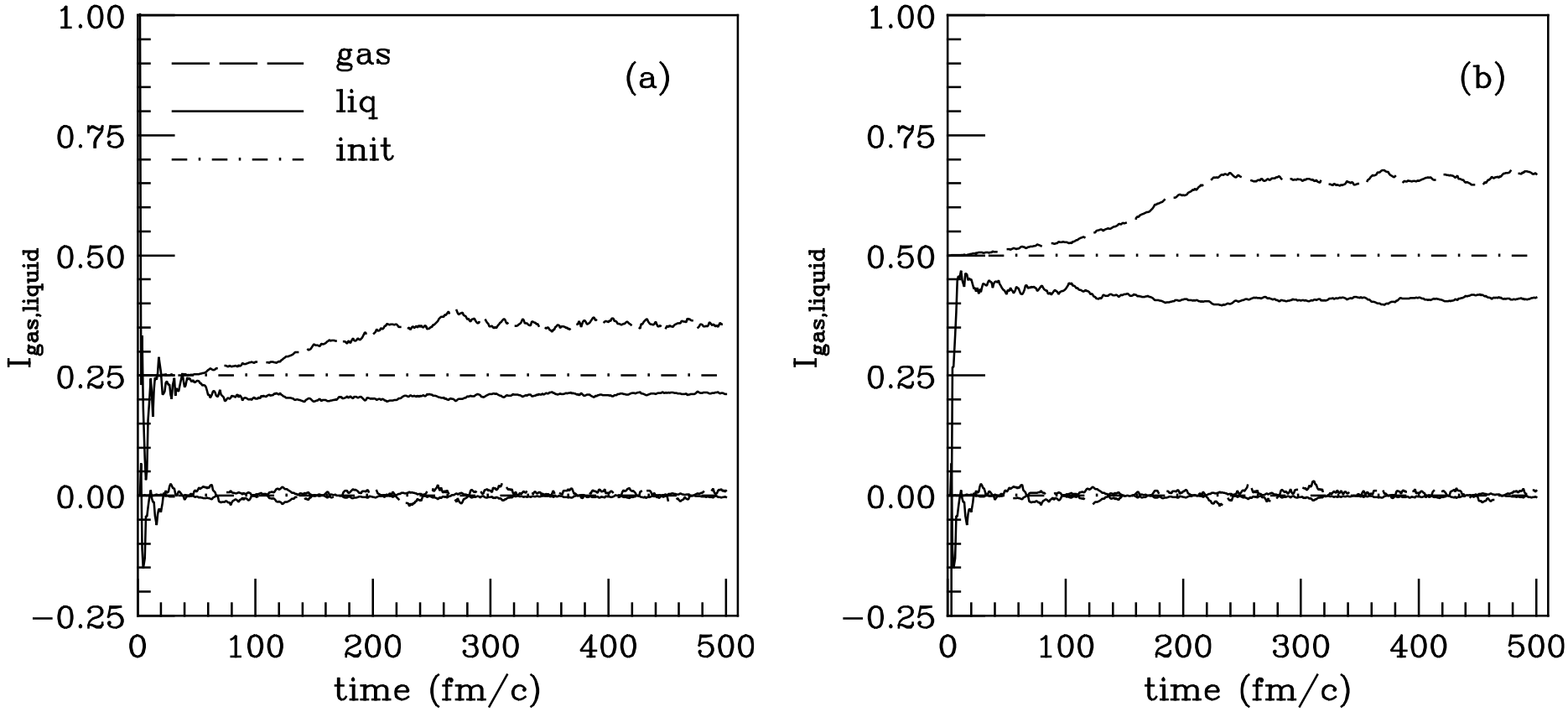
1.00
0.75
0.50
0.25
0.00
−0.25
$I_{gas,liquid}$
gas
liq
init
(a)
0
100
200
300
400
500
time (fm/c)
1.00
0.75
0.50
0.25
0.00
−0.25
$I_{gas,liquid}$
(b)
0
100
200
300
400
500
time (fm/c)

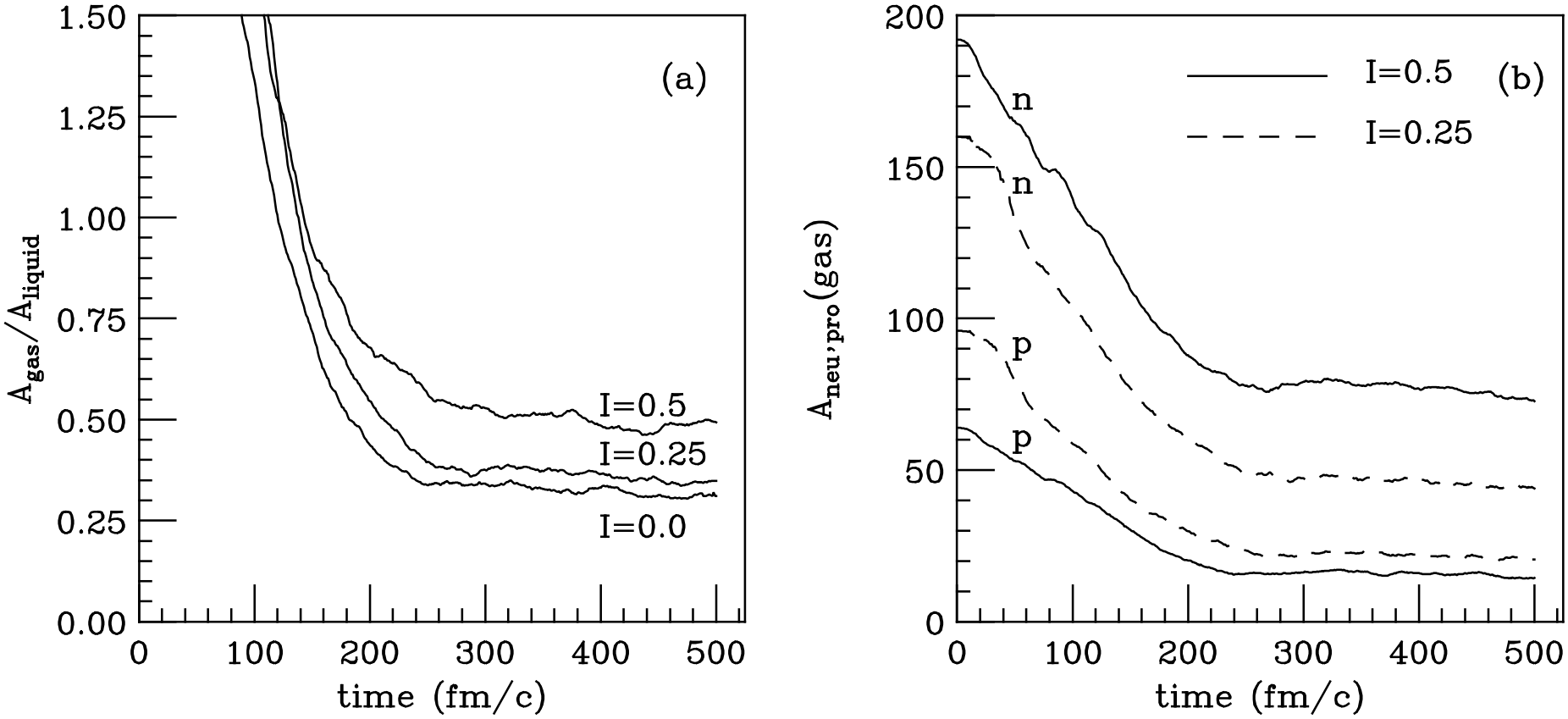
(a)
A_{gas}/A_{liquid}
1.50
1.25
1.00
0.75
0.50
0.25
0.00
0
100
200
300
400
500
time (fm/c)
I=0.5
I=0.25
I=0.0
(b)
$A_{neu,pro}(gas)$
200
150
100
50
0
I=0.5
I=0.25
n
n
p
p

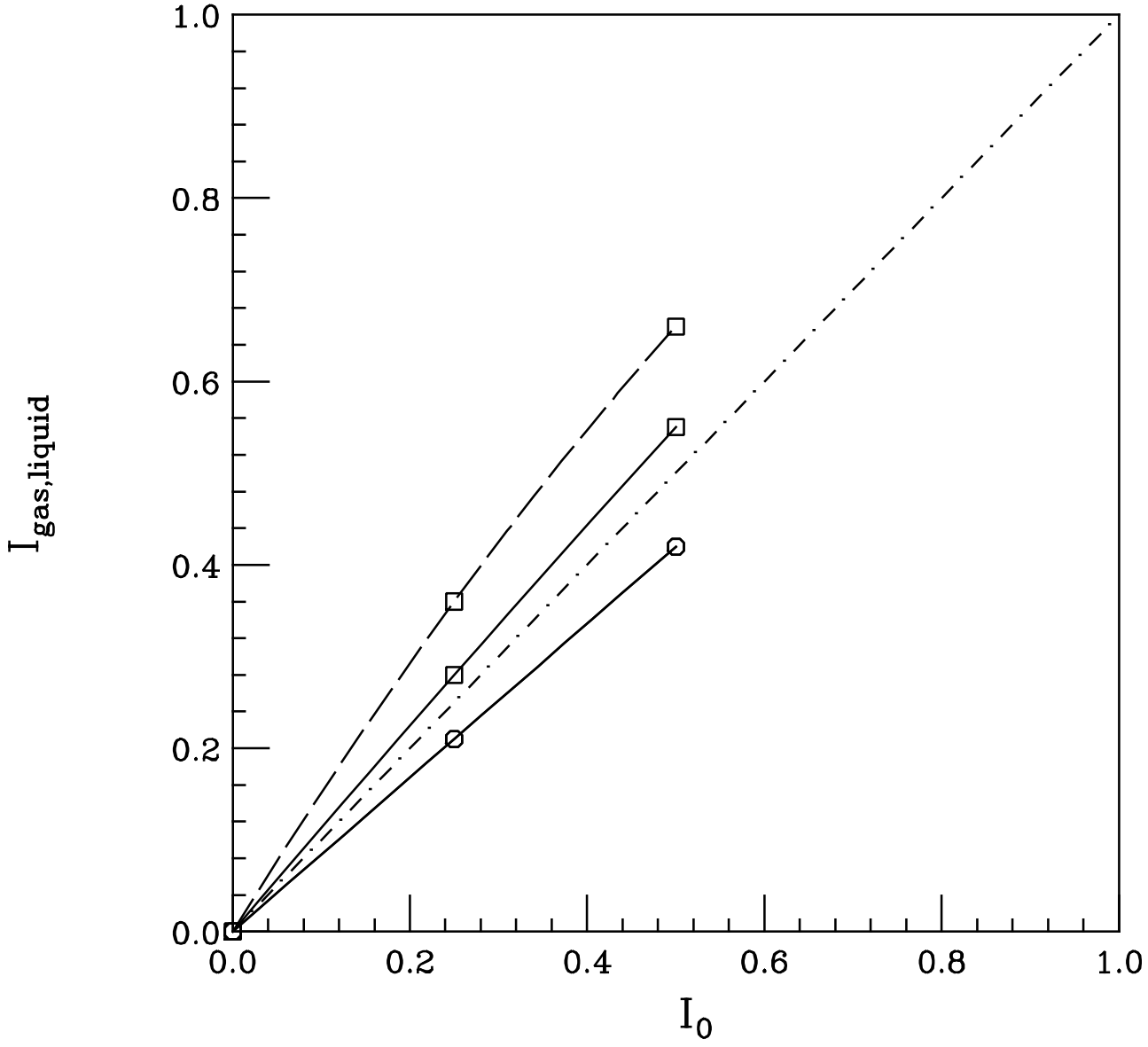
1.0
0.8
0.6
0.4
0.2
0.0
0.0
0.2
0.4
0.6
0.8
1.0
$I_{gas,liquid}$
I_0